High resolution mapping of supraglacial drainage pathways reveals link between micro-channel drainage density, surface roughness and surface reflectance.

David M. Rippin, Andrew Pomfret and Nigel King

1. Abstract

This paper reports on the use of a small unmanned aerial vehicle (sUAV) carrying a standard compact camera, to construct a high resolution orthomosaic (OM) and digital elevation model (DEM) over the lower reaches of the glacier Midtre Lovénbreen, Svalbard. Structure from Motion (SfM) techniques were used to build the OM and DEM, and together these reveal insights into the nature of supraglacial drainage. Major meandering supraglacial drainage pathways show clear dynamism, via meander cut-offs and abandoned channels. In addition, the imagery reveals a very extensive network of smaller channels that may well carry substantial amounts of water. This network of channels is in part controlled by the structure of the glacier, but in turn, these channels have a significant impact on the ice surface. Roughness of the ice surface is higher where channels are most extensive. In addition, we find a relationship between channel density and surface reflectance, such that greater channel density is associated with lower reflectance values. Given the role of surface reflectance and roughness in the energy balance of glaciers, it is therefore apparent that extensive networks of small supraglacial channels across such glaciers have the potential to have an important impact on energy exchanges between the atmosphere and the ice surface.

Keywords: *supraglacial hydrology; unmanned aerial vehicles; Structure from Motion; surface roughness*

2. Introduction

The nature and efficiency of the supraglacial drainage system of valley glaciers is of vital importance, since it is the mechanism by which water is routed across a glacier surface and ultimately delivered, via crevasses and moulins, to the glacier bed, where it can influence ice dynamics (Iken, 1981; Fountain and Walder, 1998; Campbell *et al*., 2006). Over the course of a melt-season, the density of a glacier's supraglacial channel network varies spatially and temporally as the contributing area, surface slope and water volume varies. Similarly, as melt rates change over the longer term, and as glaciers retreat and thin, such changes in supraglacial drainage are also likely to occur (Brykała, 1998; Irvine-Fynn *et al*., 2011a). These changes affect the delivery of glacier meltwater to both sub- and extra-glacial locations and, consequently, impact on glacier flow, sediment transport, and ice-flux.

Despite this obvious importance, apart from a recent modelling paper on supraglacial meandering (Karlstrom *et al*., 2013) there are only a few studies explicitly dealing with the dynamics of supraglacial drainage pathways (e.g. Knighton, 1972; Parker, 1975; Hambrey, 1977; Knighton, 1981; Marston, 1983) and many are several decades old. Given recent advances in remote sensing, new

opportunities now exist to characterise drainage at hitherto unattainable spatial and temporal resolutions.

We are also interested in the links between supraglacial channels and the roughness of a glacier's surface. Irvine-Fynn *et al*. (2011a) have proposed that microscale roughness and small-scale surface topography may be important in the inception and routing of water in small channels, but we hypothesise that in addition, the flow of supraglacial water across the ice surface may actually have an important role in controlling surface roughness itself. This link is important because surface roughness has a fundamentally key part to play in the energy balance that controls glacier melt rates, and so it impacts on glacier mass balance (Cathles *et al*., 2011). A rougher surface enhances melt rates because of its impact on turbulence in the boundary layer, thus affecting latent and sensible heat transfer. Additionally, a rougher surface enhances melt rates because energy that is reflected off a rough surface can be absorbed by another part of the ice surface. In contrast, where a surface is entirely smooth, reflected energy is lost back to the atmosphere (Cathles *et al*., 2011). Cathles *et al*. (2011) also raised concerns about the way that such topography/roughness might impact on shading and also albedo, and thus further impact on the energy balance – a relationship that needs further exploration.

In this paper, a digital camera mounted to a small unmanned aerial vehicle (sUAV) is used to gather hundreds of high-resolution digital images of the supraglacial drainage network on the glacier Midtre Lovénbreen, Svalbard, in order to gain a better understanding of supraglacial drainage behaviour. In particular, the focus is the role of supraglacial hydrology in modifying both surface roughness and impacting on surface reflectance, and therefore having a previously unacknowledged role in the energy balance of glaciers.

3. Field site and polythermal hydrology

Our work is focussed on Midtre Lovénbreen – a polythermal glacier in Svalbard (Figure 1). Polythermal glaciers are common in the Arctic, and consist of some combination of warm and cold ice. Warm ice exists very close to the pressure melting point (pmp) whereas cold ice is well below the pmp (Hodgkins, 1997; Rippin *et al*., 2011). The extensive cold ice common to polythermal glaciers means they are less dynamic and exhibit few surface crevasses (which would enable access to englacial locations). As a consequence, supraglacial channels tend to be widespread, draining water from a wide area. Melt-rates are generally low, helping with longer-term stream stability so substantial supraglacial channels can form significant elements of the polythermal drainage system. Nevertheless, small changes in meltwater production can result in substantial changes in channel walls, and meanders are common, with the ability to migrate and evolve as the ice surface changes and as discharge volume is modified (Irvine-Fynn *et al*., 2011a; Karlstrom *et al*., 2013).

Compounding the lack of studies of modern supraglacial drainage, investigations of such pathways on polythermal glaciers are extremely rare, despite them being ideal natural laboratories for such investigations. There is an even greater need for an enhanced understanding here following the identification of 'cut and closure' drainage pathways by which englacial channels have been shown to evolve from supraglacial channels in polythermal glaciers (Röthlisberger and Lang, 1987; Fountain and Walder, 1998; Vatne, 2001; Gulley *et al*., 2009). Although not the primary focus of our work,

this is important because it provides a mechanism for routing surface water to englacial and ultimately subglacial locations on polythermal glaciers, without the need for crevasses to facilitate access, which are conventionally thought to be vital.

4. Technological background

In this paper, a small unmanned aerial vehicle (sUAV) is utilised to explore supraglacial drainage. This choice is motivated by the ability to produce high resolution products at comparatively low cost, compared with manned aircraft. The approach, while still comparatively new, is slowly seeing increasing use in the earth sciences (e.g. d'Oleire-Oltmanns *et al*., 2012; Hugenholtz *et al*., 2012; 2013; Kääb *et al*., 2013) and the beginnings of its deployment in glaciological studies (e.g. Whitehead *et al*., 2013). sUAVs, coupled with increasingly compact and high-quality digital cameras, represent a potentially revolutionary tool for providing comparatively cheap high resolution aerial imagery.

While sUAVs provide the platform for data collection, it is the application of the Structure from Motion (SfM) approach to produce 3D terrain models that is primarily of benefit in the earth sciences. The technique is discussed elsewhere in more detail (e.g. James and Robson, 2012; Fonstad *et al*., 2013; Kääb *et al*., 2013, and in much detail in Snavely *et al*., 2006; 2008), but briefly, the approach relies on using views of an object or scene captured in conventional digital photographs from multiple camera positions. These images are then used to recover both camera positions and to build point-clouds of individual landscape features in three-dimensional space (cf. Westoby *et al*., 2012). From these point clouds, perfectly co-registered digital elevation models (DEMs) and orthomosaics (OMs) can be created.

5. Aims

Here, we utilise a sUAV and SfM to map the supraglacial drainage network of Midtre Lovénbreen. We do this in order to address a number of aims:

1) To better understand the way in which water is routed across polythermal glaciers.
2) To consider how this water-routing evolves through time.
3) To investigate the role of supraglacial drainage in modifying surface roughness and surface reflectance.
4) To evaluate the use of sUAVs and SfM approaches for mapping glacier hydrology, and the unprecedented insights this provides.

This investigation is important because the hydraulic behaviour of supraglacial drainage on polythermal glaciers is poorly understood and has received very little attention to date (Irvine-Fynn *et al*., 2011a). However, such drainage pathways are deserving of much more attention because of their importance in transporting water across glacier surfaces, and because of their role in energy exchanges at the surface. Surface water pathways also operate at a range of scales, and due to a lack of high resolution surface data, those pathways at the smaller scale have not previously been studied. It is our intention in this paper to redress this.

6. Methodology

In August/September 2013, a QuestUAV 200 (http://www.questuav.com/) system was deployed to survey the snout of the glacier Midtre Lovénbreen (Figure 1). The QuestUAV 200 system consists of a fixed-wing aircraft made of high density EPP (expanded polypropylene) with a wingspan of ~1.4 m. Its total weight is ~3.5 kg and it has an operating speed of 12-25 m s^{-1}. Its robust but lightweight construction means that it is able to withstand considerable impact on landing – a significant benefit as the system has no undercarriage and so 'belly-landings' must be employed on rough proglacial terrain.

The system also consists of an on-board GPS and auto-pilot which means that it can follow a pre-programmed flight plan. Full manual control is also possible in the event of unforeseen events requiring emergency manual take-over, but in addition, landing is also undertaken manually. Finally, the UAV carries a Panasonic Lumix DMC-LX5 compact digital camera, which was fixed at a focal length of 24 mm. The camera is triggered by an on-board computer to collect a JPEG image every 2 seconds.

In this paper, we report on just a single survey-flight, lasting ~15 minutes and covering > 13 km distance. 423 images were collected with an along-track overlap of 60% and a sidelap of 30% over 15 cross-glacier survey lines (Figures 1 and 2). Overlap was necessary to ensure that each point was imaged in multiple photographs. As explained above, this is fundamental to successful application of the SfM approach, and achieving such overlap, as well as sufficient spatial coverage of the study area, are the two main drivers guiding flight-planning. The sUAV flew at an altitude of ~121 m (400 ft) above the local terrain. However, as we were forced to launch our sUAV from within the forefield of Midtre Lovénbreen, and fly cross-glacier survey legs, it was necessary to gradually increase the aircraft altitude so as to maintain terrain clearance. This resulted in some complex flight-planning. One might also expect that some difficulties might arise in matching imagery due to the varied altitude of data-collection. However, no such difficulties were encountered.

Agisoft Photoscan (http://www.agisoft.ru/) was used to produce a dense point cloud from 423 images, and from this an OM was produced. The EXIF data associated with each image is used automatically within the software to estimate the field of view. Additionally, each photograph also has associated with it acquisition-coordinates and a measure of altitude, pitch, roll and yaw, all derived from the sUAV's on-board navigation system. These data assist with image-matching within Photoscan and also with geo-locating the resultant OM (and DEM). To better locate the imagery, eight markers were also positioned around the glacier margin before the survey flight. A Trimble R6 dGPS system was used to accurately locate these ground control points (GCPs). Point locations were processed against a permanent GPS base station located in Ny-Ålesund, and operated as part of the EUREF Permanent GNSS Network (http://www.epncb.oma.be/). Unfortunately, only four of these GCPs were visible in the imagery, and due to logistical constraints and other limitations, all these markers were located in front of the glacier snout. Nevertheless these were used, along with the 423 image GPS coordinates, to accurately locate the images and resultant OM in real space. Photoscan was then used to produce a high resolution digital elevation model (DEM) of the ice surface (10 cm grid-cells), alongside the OM (5cm grid-cells) and the OM and DEM were exported and uploaded into the open source GIS package: QGIS.

The day after the glacier survey, 128 on-ice check-points were collected using the Trimble dGPS system (Figure 1). Each 'check-point' simply consisted of a point measurement of easting, northing and ice surface elevation, and these were used to check the accuracy of the SfM-derived DEM. Over these 128 points there was a root mean square (RMS) error of 1.49 m between these spot-derived dGPS elevations and elevations from the SfM derived DEM (mean absolute mismatch in elevation was 1.05 m). Errors were considerably worse upglacier, away from our GCPs, than they were in the lower reaches of the glacier, close to our GCPs (see Figure 1b). However, despite this, there was an exceptionally good linear relationship between the dGPS-derived and SfM-derived elevations (R^2 = 0.9999; Figure 1c). The relationship between the dGPS points and the raster elevation was therefore used to linearly tune the SfM-derived DEM to our dGPS-surveyed points. We recognise there are limitations in doing this, but given the very high quality of fit, we deemed this to be an acceptable procedure to follow. In doing so, the RMS error was reduced to 0.40 m at these 128 comparison-locations (mean absolute error of 0.35 m).

Our DEM was also compared with a lidar-derived DEM based on airborne lidar (light detection and ranging) data collected in 2005, as reported by Arnold *et al*. (2006), Barrand, (2007), Barrand *et al*. (2009) and Irvine-Fynn *et al.* (2011b), with a spatial resolution of 2.5 m. The results of this comparison are described below.

In addition, various products from the DEM and OM were derived. Firstly, surface roughness was calculated. In order to ensure that large-scale topography did not dominate the roughness signal, this was removed by detrending the DEM (following Shepard *et al*., 2001). This process was optimised by using a smoothing window that ensured that the mean of the residuals surface was as close to zero as possible. Experimentation revealed a ~2.5 m long smoothing window to be optimum. Then, standard deviation was used as a proxy for surface roughness. Roughness can be expressed as vertical variation over a given distance (Rippin *et al*., 2011) and so it is important to consider a range of window sizes over which the roughness value is determined. Increasing the window size has the effect of decreasing the variability in the roughness output – i.e. smoothing the output. Roughness was then explored over windows of 2.5 m, 10.5 m, 20.5 m and 40.5 m.

Secondly, a proxy for albedo was determined by exploring surface reflectivity from the OM. A standard digital photographic image is not a true measure of albedo, however, following Corripio (2004), the assumption was made that there is a direct relationship between the signal recorded by a camera and surface albedo or reflectance. Furthermore, this assumption is additionally justified because most of the energy reflected by many materials, including snow, is in the visible portion of the electromagnetic spectrum (Corripio, 2004; Westoby, 2009). Values of emissivity in each of the red, green and blue bands of the OM image were extracted, before summing these for each pixel to give a proxy for surface reflectance. These were then averaged over 10 m cells.

Finally, the density of supraglacial channels was quantified. Channels are so extensive across the surface of Midtre Lovénbreen that manually mapping them proved to be an impossible task. Several approaches for isolating channel locations were explored as follows:

1) ***Using surface reflectance*** since this is generally lower where flowpaths are observed. However, given the desire to actually assess the significance of drainage on surface reflectance, such an approach is circular and so it was rejected.

2) ***Using a modelling approach***, whereby theoretical drainage pathways were determined using the DEM, by assuming that water is generated in every cell across the glacier surface (cf. Shreve, 1972). Water flow was then modelled using a flow accumulation approach in which it is assumed that all water from an upstream cell passes to the most downhill adjacent cell, and so the accumulation volume totals are summed (cf. Rippin *et al*., 2003). Such approaches are commonplace (cf. Arnold *et al*., 1998; Banwell *et al*., 2012) and here resulted in channels that very accurately followed observed pathways. However, it was noted that there is a tendency to over-produce hydrological pathways where there are none in reality.
3) ***Using the detrended DEM***, in which large-scale topography has been removed, and employing an iterative approach so as to arrive at an elevation threshold in which channels (trough-bottoms) are isolated from the rest of the terrain. This led to true channel locations being identified with acceptable accuracy.

It is this third method that was carried forward. In doing so, calculated channel density, or rather the frequency with which channels appeared in 20 m grid-cells was determined.

The outcomes of these studies are discussed below, with respect to three distinct and broad themes. Under each theme, we first briefly address the state of knowledge before presenting our results and interpreting them.

7. The proglacial area

7.1. State of knowledge

In the forefield, braided river systems, meltwater ponds, and substantial debris ridges and moraines are present and are easily identified. These features also manifest themselves as subtle changes in elevation. It is here, in the forefield, where we attempted to compare our output with those of the 2005 lidar survey mentioned previously (Arnold *et al*., 2006; Barrand, 2007; Barrand *et al*., 2009 and Irvine-Fynn *et al*., 2011b). This area is marked by a lack of bedrock features, and so it proved to be impossible to identify features where no change in elevation might be expected. This is of particular relevance because Irvine-Fynn *et al*. (2011b) specifically report on changes in the elevation of the forefield due to sediment redistribution. They identified two primary drivers of sediment reworking: (i) active fluvial incision by proglacial streams and (ii) downwasting of lateral moraines related to the melting of contained ice-cores and coupled mechanical processes. Across the whole of the studied forefield, Irvine-Fynn *et al*. (2011b) noted an annual surface lowering of 0.05 ma^{-1} ± 0.2, with maximum lowering to be found on the western moraine ridge where ice-core melting was significant (0.65 ma^{-1} ± 0.2; their zone iii) and in active proglacial streams (0.13 ma^{-1} ± 0.2; their zone iv) where fluvial incision was significant.

7.2. Results

The proglacial landscape features identified above are clearly visible in the OM and corrected DEM, produced using the SfM technique (Figure 2). The detail inherent in this imagery is spectacular, and interactive exploration of the imagery reveals astonishingly high resolution detail.

Similar to Irvine-Fynn *et al*. (2011b), we too identified substantial lowering of the proglacial area over the 8 year period between this earlier lidar survey and our own work, although our survey only covers small parts of the proglacial and marginal area. In these same regions, we find an average annual surface lowering of the western moraine ridge of 1.12 ma^{-1}, although there was substantial variability amongst these values. Further, in the zone iv of Irvine-Fynn *et al*. (2011b) we identify a mean surface lowering of 0.24 ma^{-1}.

7.3. Discussion

Both the work of Irvine-Fynn *et al*. (2011b) and ourselves showed that much of the forefield lowered, with only small areas showing virtual stability. Our measurements are clearly larger, but we do not consider that the discrepancy between ours and the older measurements are a significant cause for concern as there are clear geomorphological explanations for this. Irvine-Fynn *et al*. (2011b) had only 23 months between two consecutive lidar surveys, from which to draw their conclusions, whereas we had 8 years. Over this longer period, on the western moraine ridge, it is highly likely that larger-scale mass-movement processes such as slumping or sliding of moraines may occur as the ice-core melts out more substantially, and it is this to which we attribute the larger value we record. With regards to the zone iv of Irvine-Fynn *et al*. (2011b), our values are again greater, but it is worth highlighting the large error estimates in their study, and again the fact that their measurements are based on a relatively short time-period. Over the 8 years between the surveys we utilise, substantial changes could have taken place, perhaps related to fluvial incision, melting of ice-cores or mass movements, thus explaining the larger values we observe.

Despite the discrepancies, we are encouraged that our UAV-derived DEM is certainly comparable to that derived by lidar, although more extensive and spatially distributed ground control points are desirable. These are, however difficult to obtain in terrain such as we encountered, where even the forefield shows substantial displacement as we have demonstrated. These observations and conclusions regarding difficulties associated with constraining magnitudes of surface change are not the focus of our work, and so absolute elevation values are also not fundamental. The remainder of this study focusses on changes on the surface of Midtre Lovénbreen regarding surface hydrology.

8. Supraglacial hydrology

8.1. State of Knowledge

The presence of widespread meander cut-offs and abandoned channel sections on the surface of glaciers can, we suggest, be interpreted as being indicative of substantial supraglacial channel dynamics. This is because, in the first instance, as with meandering in alluvium, meander cut-offs clearly indicate that streams are continually eroding their banks such that the two closest part of a bend connect, thus eliminating the need for water to follow the more tortuous meander. However, despite meander cut-offs being commonly observed in alluvium (e.g. Allen, 1965; Hooke, 1997; Knighton, 1998; Thompson, 2003), they have only briefly been mentioned in the glaciological literature before (Hambrey, 1977; Knighton, 1981; Marston; 1983) and nowhere, to our knowledge, have they been revealed in the detail that we are able to provide. However, in the limited glacier-focussed studies to date, it is important to note that Marston (1983) reports on a different

mechanism behind the construction of such abandoned meander loops (cf. Irvine-Fynn *et al*., 2011a). Here, instead of 'pinched off' meander loops, formed due to lateral meander evolution, apparently entirely abandoned loops, disconnected from the main channel may exist. Marston (1983) states that such features are a product of rapidly downcutting channels in which cut-offs occur because of vertical abandonment. In this way, such channels effectively become englacial as meanders are abandoned – an effect known as 'cut and closure' and reported previously (cf. Röthlisberger and Lang, 1987; Fountain and Walder, 1998; Vatne, 2001; Gulley *et al*., 2009).

We also propose that further channel dynamism can be inferred from the presence of abandoned channel sections (i.e. regions that are clearly water-formed, but which currently do not carry water). Such avulsion is usually attributed to: (i) a change in the surface slope of the existing channel (normally due to a decrease in channel gradient); (ii) a change in the surface slope of the avulsion course (normally due to an increase in the gradient away from the older channel); or (iii) a reduction in the capacity of the older channel to carry the provided sediment and water load (Jones *et al*., 2009). Avulsion of supraglacial channels has not previously been discussed in this way (although the term avulsion has, however, been used to explain the construction of vertically abandoned meander loops on glaciers, as discussed above) but it seems highly likely that some combination of all these processes is responsible. This is because local changes in surface gradient are easily achieved through a melt-season, due to differential ablation over an ice surface. Similarly, changes in the capacity of existing channels are also easily explained, since as meteorological conditions vary over a range of timescales, the amount of meltwater generated at the ice surface will vary. Additionally, relatively rapid melting out of meander channels may occur if channel walls are preferentially melted. Such evidence of avulsion, and indeed the abandonment of substantial reaches of channel, also indicates a very dynamic system.

8.2. Results

Midtre Lovénbreen is deeply incised by two very prominent primary supraglacial streams (Figure 2) – an eastern and western stream. The term 'primary' is introduced here to distinguish them from an additional extensive, much finer, supraglacial network that is discussed below. These primary supraglacial streams are exceptionally pronounced and clearly visible in both the OM and DEM (Figure 2). Close inspection of both the OM and DEM reveals that as well as the prominent meandering of both the eastern and western primary streams, there is also substantial evidence of the dynamic behaviour inherent within them, as introduced above (Figure 3).

In our high-resolution imagery, we identify areas where sections of channel (although not necessarily entire meanders) apparently disappear, and reappear further downglacier (Figures 3g and h) which we interpret as being a consequence of such vertical abandonment. These meander cut-offs are best revealed in the OM imagery (Figure 3a), and appear as regions with subtly different surface texture (Figure 3b). Additionally, the high resolution of the OM and DEM helps to identify substantial abandoned channel sections (Figure 3c and d). These features have widths of ~1-1.5 m and so it is only with such high resolution imagery as presented here, that these features are visible.

We also identify an extensive network of much smaller channels which we term a 'micro-channel network'. This complex and intricate secondary supraglacial drainage network consists of an intricate system of branching micro-channels, just a few centimetres to tens of centimetres wide, and therefore much smaller than the larger, primary supraglacial channels. These secondary

channels are visible at unprecedented resolution in our high resolution OM and DEM. There are two types of micro-channels – those that exist as parts of anabranching networks and which may exhibit some subtle meandering; and those that appear primarily structural – i.e. they are exceptionally straight and thus must owe their origins to structural features. Cutting across these micro-scale channels are other perpendicular features that are also likely structural. These cross-flow features only act as partial routeways where sub-parallel routeways cross them, and where for short distances they transmit water.

8.3. Discussions

In our imagery, substantial channel dynamism is clear. These observations are an intriguing and important addition to the fairly sparse literature on supraglacial drainage, expanding substantially what is already known. For instance, very recently, Karlstrom *et al*. (2013, p1897) stated that 'although there is likely to be some inheritance of large channels from year to year, supraglacial hydrology re-evolves from initial channelization to large-scale organization each year as surface melting waxes and wanes'. Our work broadly supports these findings, in that we identify both persistent, deeply incised channels and a more temporary but widespread network of smaller channels. The deeply incised supraglacial channels discussed above, are clearly reused year after year. We know these channels are re-used from personal observations, and it has also been reported by Irvine-Fynn *et al*. (2011a). Observation of persistent, inherent channels are not new. Hambrey (1977) reported that where there is a low activity index (i.e. low accumulation and ablation), channels can persist year after year (cf. Glen, 1941). On Midtre Lovénbreen, we have observed that these primary meandering channels become filled with snow over the course of the winter, but once water begins to flow in the melt season, it is channelled to these primary routeways and flow continues.

The micro-channel network seems likely to be re-initiated annually (Figures 3e and f). The extensive cold ice that is common in polythermal glaciers means they are less dynamic and exhibit fewer surface crevasses (which would enable access to englacial locations) than temperate glaciers (Etzelmüller *et al*., 1993; Irvine-Fynn *et al*., 2011a). As a consequence, supraglacial channels tend to be more widespread than on temperate glaciers, draining water from a wider area. Melt-rates that are generally lower than on temperate glaciers also help with longer-term stream stability so that substantial supraglacial channels can form significant elements of the polythermal drainage system (cf. Hambrey, 1977; Irvine-Fynn *et al*., 2011a). Rather than water moving in a sheet, these incised micro-channels appear to be the dominant form of drainage across much of the glacier, before routing water to the meandering network. Such networks have been reported briefly before. Hambrey (1977) identified rill-like features on the surface of Charles Rabots Bre, Norway, and suggested that the orientation and location of this drainage network might be controlled by structures within the ice such as longitudinal foliation and the boundaries of discrete flow units (cf. Hambrey *et al*., 2005). Furthermore, Irvine-Fynn *et al*. (2011a) in their review of polythermal glacier hydrology, report on the work of Kostrzewski and Zwolinski (1995) and their observations of dendritic surface drainage. Here there are hints of previously elevated glacier dynamism – the perpendicular features we identify are likely structural (e.g. transverse fractures and crevasse traces as identified by Hambrey *et al*. (2005), and representative of a more dynamic phase in the glacier's history).

9. Controls on surface roughness

9.1. State of Knowledge

Arnold *et al*. (2006) explored the role of topography on the energy balance of Midtre Lovénbreen. However, although nominally an investigation of roughness at the 'small scale', this work actually dealt with topographic features of less than ~ 100 m, and was derived from a DEM that although generated from airborne lidar data with a spatial resolution of 0.7-1.5 m, were used to produce a 20 m DEM. They concluded that topography plays a vital role in controlling shading, which impacts melt rates over an ice surface directly, and through various feedbacks (Arnold *et al*., 2006). More recently, Cathles *et al*. (2011) have also discussed the role of surface drainage features on surface roughness, although the primary focus of their work was on drained features and whether solar radiation can enlarge them and impact on the movement and storage of surface water. This was a modelling study dealing with quite large features – idealised crevasses and canyons with an initial width of 5 m. The data we present here is therefore important because we are able to explore surface roughness considering features that are just a few centimetres in diameter.

9.2. Results

The extensive network of micro-scale channels is visible in the OM and the DEM, and the presence of these surface channels suggests high frequency, low amplitude surface roughness. We explored roughness over windows of 2.5 m, 10.5 m, 20.5 m and 40.5 m, finding that the general signal was similar in all cases, with a window of 20.5 m providing the optimum balance of detail, yet revealing generalised patterns that are not masked by extreme values. Nevertheless, very high roughness values dominate around the major supraglacial channels. Masking these out (see Figure 4) reveals that roughness is variable across much of the glacier, however, there is an area of broadly elevated roughness in the eastern upglacier sector, and another similar area in the central-lower sector. Conversely, low roughness values dominate in the upper central and western sides of the glacier, and indeed along the full length of the glacier's western side.

Although true measurements of albedo from the imagery presented here are beyond the scope of this work, it is possible to identify differences in surface reflectivity. This takes the form of both differential debris cover, but also distinct reflectivity variations visible along drainage routeways (see Figure 5) not obviously related to debris cover. It is possible that these variations along channels reflect the manifestation of shading on channel walls, or the presence of water in these channels. Clearly, the precise control and significance needs further investigations, but here, we present surface reflectivity as a proxy for albedo. Figure 5 shows that as with measurements of roughness, there is significant variability in proxy-reflectance values. Reflectance values are unsurprisingly lowest in the heavily debris-covered margins. However, beyond this, reflectance is lowest in the eastern upglacier sector, where roughness is highest. Reflectance is moderately high in the central part of the glacier, and there is a large low-high-reflectance region along the glacier's western side (as well as other smaller patches elsewhere in the lower reaches).

Finally, channel density was explored (Figure 6). Most prominently, channel density is highest at the eastern margin, but also moderately high in the eastern upglacier region. There is also a moderately

dense region in the lower-central region and a large area of low channel density in the western lower-glacier sector, and in part along the western margin.

9.3. Discussions

There is clearly some relationship between roughness and reflectance, such that higher roughness regions are associated with lower reflectance, while low roughness regions are associated with higher reflectance. We do, however, encourage some caution in interpreting these results as patchy low-cloud visible in some of our imagery may be responsible for some of the apparent variations in surface reflectivity.

Furthermore, there is also a striking correspondence between the roughness and reflectivity maps and channel density, such that generally rough areas are associated with high channel density and low reflectance, whereas smooth areas are associated with lower channel density and higher reflectance. This work therefore not only identifies an extensive and widespread micro-channel network, but also that this there are feedbacks between this network, surface roughness and likely differential energy exchanges between the glacier and the atmosphere. The resolution of our imagery also means that such feedbacks needs to be (and indeed can be) considered at spatial scales not previously considered. We propose that the micro-channel drainage network is both controlled by, and controls surface roughness through the role of water in controlling spatially variable surface melt rates. Unsurprisingly then, where channel density is greater, the surface is rougher, and we also see a correspondence between surface reflectance and channel density.

10. Conclusion

We deployed a QuestUAV 200 in Svalbard and succeeded in gathering exceptionally high resolution aerial imagery over the glacier Midtre Lovénbreen. Using Structure from Motion, this imagery was used to create a composite high resolution orthomosaic and digital elevation model with spatial resolution of 5 cm and 10 cm respectively. The detail in this imagery is extraordinary, and as well as a wealth of information on ice structure, there is a great amount of detail apparent with regards to supraglacial hydrology. This is an often overlooked area of glaciology, and so applying modern observational approaches has allowed new insights to be gained. Our imagery reveals discrete, flow parallel supraglacial channels that exhibit intense meandering. These primary supraglacial routeways are evidence of long term supraglacial drainage stability, but also provide evidence of significant dynamism, through clear evidence of meander cut-offs and abandoned channel reaches. In addition, there is an extensive, near-glacier-wide network of secondary micro-scale drainage routeways, transporting water in a branching channel network, controlled in part by glacier structure. This extensive supraglacial drainage network has a previously overlooked role to play in determining the roughness of an ice surface and thus in the energy balance. The effect is likely to be most pronounced in environments where supraglacial drainage is extensive due to a lack of crevasses to divert water internally. Therefore, it is on polythermal glaciers where the effect is of greatest importance. As climate continues to warm and Arctic glaciers respond, it is likely that supraglacial drainage during the melt-season will become more extensive and more intense, with an equivalent impact on surface roughness. This has implications for the energy balance via the direct role on roughness, but also through the impact on surface reflectivity. The precise importance of

this, in the way that glaciers respond, remains to be determined and is beyond the scope of this paper, but it is proposed that determining the role of evolving surface roughness on the energy balance needs further exploration.

These new insights have been achievable because of the extraordinarily high resolution imagery that sUAVs and SfM provide. This is therefore an important new tool in glaciology, and there is great potential to achieve similar insights in other areas of glaciology.

Acknowledgements

Funding in support of this work was provided by the University of York. We thank Nick Cox of the NERC Arctic Research Station for support while conducting fieldwork. We thank Professor Michael Hambrey for useful discussions on an early draft of this paper, and similarly useful insights on a later version from Dr Duncan Quincey. We thank QuestUAV and their staff for their assistance and guidance and Dr Neil Arnold for access to the 2005 surface DEM. We also thank two anonymous referees as well as the Associated Editor and Editor for insightful comments that have helped to improve this paper.

References

Allen, J.R.L. 1965. A review of the origin and characteristics of recent alluvial sediments. *Sedimentology*, **5**, 89–191.

Arnold, N., K. Richards, I. Willis and M. Sharp. 1998. Initial results from a distributed, physically based model of glacier hydrology. *Hydrological Processes*, **12**(2), 191-219.

Arnold, N.S., W.G. Rees, A.J. Hodson and J. Kohler. 2006. Topographic controls on the surface energy balance of a high Arctic valley glacier. *Journal of Geophysical Research*, **111**(F2), F02011. (10.1029/2005JF000426.)

Banwell, A.F., N.S. Arnold, I.C. Willis, M. Tedesco, A.P. Ahlstrom. 2012. Modeling supraglacial water routing and lake filling on the Greenland Ice Sheet. *Journal of Geophysical Research – Earth Surface*, **117**, F04012, DOI: 10.1029/2012JF002393.

Barrand, N.E. 2007. *Changes in volume and extent of NW Svalbard glaciers using airborne lidar and digital photogrammetry*. Ph.D. Thesis, Dept. of Geography, Swansea University, Swansea, Wales.

Barrand, N.E., T.M. Murray, T.D. James, S.L. Barr and J.P. Mills. 2009. Optimising photogrammetric DEMs for glacier volume change assessment using laser-scanning derived ground control points. *Journal of Glaciology*, **55**(189), 106-116, doi: 10.3189/002214309788609001

Brykała, D. 1998. Evolution of supraglacial drainage on Waldemar Glacier (Spitsbergen) in the period 1936–1998, in: *Polish Polar Studies: 25th International Polar Symposium*, 247–263, Inst. Geofiz. PAN, Warsaw.

Campbell, F.M.A, P.W. Nienow and R.S. Purves. 2006. Role of the supraglacial snowpack in mediating meltwater delivery to the glacier system as inferred from dye tracer investigations. *Hydrological Processes*, **20**(4), 969-985.

Cathles, L.M., D.S. Abbot, J.N. Bassis and D.R. MacAyeal. 2011. Modeling surface-roughness/solar ablation feedback: application to small-scale surface channels and crevasses of the Greenland ice sheet. *Annals of Glaciology*, **52**(59), 99-108.

Corripio, J. 2004. Snow surface albedo estimation using terrestrial photography. *International Journal of Remote Sensing*, **25**(24), 5704-5729.

d'Oleire-Oltmanns, S., I. Marzolff, K.D. Peter and J.B. Ries. 2012. Unmanned Aerial Vehicle (UAV) for monitoring soil erosion in Morocco, Remote Sens., 4, 3390–3416.

Etzelmüller, B., G. Vatne, R.S. Ødegåed and J.L. Sollid. 1993. Dynamics of two subpolar valley glaciers, Erikbreen and Hannabreen, Liefdefjorden, northern Spitsbergen. *Geografiska Annaler*, Ser. A, **75**(1-2), 41-54, doi:10.2307/521052.

Fonstad, M.A., J.T. Dietrich, B.C. Courville, J.L. Jensen and P.E. Carbonneau. 2013. Topographic structure from motion: a new development in photogrammetric measurement. *Earth Surface Processes and Landforms*, **38**, 421-430.

Fountain, A.G. and J.S. Walder. 1998. Water flow through temperate glaciers. *Reviews of Geophysics*, **36**(3), 299-328.

Glen, A.R. 1941. A sub-arctic glacier cap: the West Ice of North East Land. *Geogr. J.*, **98**, 65-76 and 135-146.

Gulley, J. D. *et al*. 2009. A cut-and-closure origin for englacial conduits in uncrevassed regions of polythermal glaciers. *Journal of Glaciology*, **55**(189), 66–80, doi:10.3189/002214309788608930.

Hambrey, M.J. 1977. Supraglacial drainage and its relationship to structure, with particular reference to Charles Rabots Bre, Okstindan, Norway. *Norsk Geografisk Tidsskrift - Norwegian Journal of Geography*, **31**(2), 69-77.

Hambrey M.J., T. Murray, N.F. Glasser, A. Hubbard, B. Hubbard, G. Stuart, S. Hansen and J. Kohler. 2005. Structure and changing dynamics of a polythermal valley glacier on a centennial timescale: Midre Lovénbreen, Svalbard. *Journal of Geophysical Research*, **110**, F01006. DOI: 10.1029/2004JR000128.

Hodgkins, R. 1997. Glacier hydrology in Svalbard, Norwegian High Arctic. *Quaternary Science Reviews*, **16**, 957-973.

Hooke, J. M. 1997. Styles of Channel Change, pp 237–268, in C. R. Thorne, H. D. Hey, and M. D. Newson (eds.) Applied Fluvial Geomorphology for River Engineering and Management. John Wiley & Sons, New York.

Hugenholtz, C.H., B.J. Moorman, K. Riddell and K. Whitehead. 2012. Small unmanned aircraft systems for remote sensing and earth science research, Eos, Transactions American Geophysical Union, **93**, 236–236.

Hugenholtz, C.H., K. Whitehead, T.E. Barchyn, O.W. Brown, B.J. Moorman, A. LeClair, T. Hamilton and K. Riddell. 2013. Geomorphological mapping with a small unmanned aircraft system (sUAS): feature detection and accuracy assessment of a photogrammetrically-derived digital terrain model, *Geomorphology*, **194**, 16–24.

Iken, A. 1981. The effect of the subglacial water pressure on the sliding velocity of a glacier in an idealized numerical model. *Journal of Glaciology*, **27**(97), 407-421.

Irvine-Fynn, T.D.L., A.J. Hodson, B.J. Moorman, G. Vatne and A.L. Hubbard. 2011a. Polythermal glacier hydrology: a review. *Reviews of Geophysics*, **49**, RG4002, doi:10.1029/2010RG000350.

Irvine-Fynn, T.D.L., N.E. Barrand, P.R. Porter, A.J. Hodson and T. Murray. 2011b. Recent High-Arctic glacial sediment redistribution: a process prespective using airborne lidar. *Geomorphology*, **125**, 27-39.

James, M.R. and S. Robson. 2012. Straightforward reconstruction of 3D surfaces and topography with a camera: accuracy and geoscience application. *Journal of Geophysical Research*, **117**, F03017, doi:10.1029/2011JF002289.

Jones, L.S. and S.A. Schumm. 2009. Causes of avulsion: an overview, in Fluvial Sedimentology VI (eds N.D. Smith and J. Rogers), Blackwell Publishing Ltd., Oxford, UK. doi: 10.1002/9781444304213.ch13

Kääb, A., L. Girod and I. Berthling. 2013. Surface kinematics of periglacial sorted circles using Structure-from-Motion technology. *The Cryosphere Discuss*, **7**, 6043-6074.

Karlstrom, L., P. Gajjar and M. Manga. 2013. Meander formation in supraglacial streams. *Journal of Geophysical Research: Earth Surface*, **118**, 1897-1907, doi:10.1002/jgrf.20135.

Knighton, A.D. 1972. Meandering habit of supraglacial streams. *Geological Society of America Bulletin*, **83**, 201-204.

Knighton, A.D. 1981. Channel form and flow characteristics of supraglacial streams, Austre Okstindbreen, Norway. *Arctic and Alpine Research*, **13**(3), 295-306.

Knighton, D. 1998. *Fluvial Forms and Processes*. Arnold, London.

Kostrzewski, A. and Z. Zwoliński. 1995. Hydraulic geometry of a supraglacial stream. Quaestiones Geogr., **4**(special issue), 165–176.

Marston, R.A. 1983. Supraglacial stream dynamics on the Juneau Icefield. *Annals of the Association of American Geographers*, **73**(4), 597-608.

Parker, G. 1975. Meandering of supraglacial melt streams. *Water Resources Research*, **11**(4), 551–552.

Rippin, D. and 6 others. 2003. Changes in geometry and subglacial drainage of Midre Lovénbreen, Svalbard, determined from digital elevation models. *Earth Surface Processes and Landforms*, **28**(3), 273–298.

Rippin, D.M., J.L. Carrivick and C. Williams. 2011. Evidence towards a thermal lag in the response of Kårsaglaciären, Northern Sweden, to climate change. *Journal of Glaciology*, **57**(205), 895-903.

Röthlisberger, H. and H. Lang. 1987. Glacial hydrology, in: *Glacio-Fluvial Sediment Transfer: An Alpine Perspective*, edited by A. M. Gurnell and M. J. Clark, 207–284, John Wiley, Chichester, U.K.

Shepard, M.K., B.A. Campbell, M.H. Bulmer, T.G. Farr, J.R. Gaddis and J.J. Plaut. 2001 The roughness of natural terrain: a planetary and remote sensing perspective. *Journal of Geophysical Research*, **106**(E12), 32,777-32,795.

Shreve, R.L. 1972. Movement of water in glaciers. *Journal of Glaciology*, **11**(62), 205-214.

Snavely, N., S.M. Seitz and R. Szeliski. 2006. Photo tourism: exploring photo collections in 3D. *ACM Transactions on Graphics* **25**(3), 835–846.

Snavely N., S.M. Seitz and R. Szeliski. 2008. Modeling the world from internet photo collections. *International Journal of Computer Vision*, **80**(2), 189–210.

Thompson, D.M. 2003. A geomorphic explanation for a meander cutoff following channel relocation of a coarse-bedded river. *Environmental Management*, **31**(3), 385-400.

Vatne, G. 2001. Geometry of englacial water conduits, Austre Brøggerbreen, Svalbard. *Norsk Geografisk Tidsskrift*, **55**, 24–33.

Westoby, M.J. 2009. *Investigating albedo and the optical properties of supraglacial debris cover using a terrestrial photography approach: Ghiacciaio del Belvedere, Italian Alps*. MSc Thesis, Aberystwyth University.

Westoby, M.J., J. Brasington, N.F. Glasser, M.J. Hambrey and J.M. Reynolds. 2012. 'Structure-from-Motion' photogrammetry: a low-cost, effective tool for geoscience applications. *Geomorphology*, **179**, 300-314.

Whitehead, K., B.J. Moorman and C.H. Hugenholtz. 2013. Brief Communication: low-cost, on-demand aerial photogrammetry for glaciological measurements. *The Cryosphere*, **7**, 1879-1884.

Figure captions

Figure 1: Hill-shaded 2.5 m Lidar-derived DEM of Midtre Lovénbreen, based on data collected in 2005 (after Arnold, N.S. personal communication). Pale-red shaded area represents the region covered in our 2013 survey. Yellow dots represent camera locations and dark-blue dots represent on-ice check-points. Inset (a) shows the location of Midtre Lovénbreen in Svalbard. Inset (b) shows how errors between dGPS-derived on-ice check points and our DEM increase upglacier. Inset (c) shows the relationship between surface elevations derived from our SfM-produced DEM and our dGPS on-ice check-points.

Figure 2: (a) Ortho-mosaic of the lower reaches of Midtre Lovénbreen. Mosaic created from 423 separate images collected during a single UAV flight. (b) Hillshaded digital elevation model derived from ortho-mosaic with a resolution of 10 cm. Both OM and DEM reveals spectacular detail with meandering supraglacial channels clearly visible and subtle surface features. On (b), the (red) shaded area represents the region of the forefield where our DEM elevations are compared with those of Irvine-Fynn *et al.* (2011b). Elevation differences are expressed in metres per year. Positive change indicates surface lowering between 2005 and 2013. Yellow dots indicate camera locations. Red squares with letters on part (a) indicate locations of parts of Figure 3, such that 'A' indicated where Figure 3a (and associated part b) is derived from; 'C' indicates where Figure 3c (and associated part d) is derived from etc.

Figure 3: Parts a (OM) and b (DEM) show a section of the western primary channel where meander cut-offs are clearly evident. These are marked. Parts c (OM) and d (DEM) show a part of the western primary channel and an adjacent abandoned primary routeway. Parts e (OM) and f (DEM) show the extensive microchannel network. Parts g (OM) and h (DEM) show a potential region of cut-and-closure - i.e. where the ice surface has deformed over a once-supraglacial channel. Locations of each of these figures are marked on Figure 2a.

Figure 4: Surface roughness calculated as the standard deviation of detrended surface elevation in 20.5 m windows. Note how roughness is greatest in the upper-eastern reaches of the glacier, and lowest in the lower-western reaches. Background is hill-shaded topography derived from our 10 m surface DEM.

Figure 5: Surface reflectance calculated as the sum of the signal strength in the red, green and blue channels, as a crude proxy for albedo. These values were integrated over 10 m cells. Reflectance was lowest in the very lowest marginal areas (where debris cover is high). It was also low in the upper-eastern region of the glacier. Highest values are found close to the margins, particularly in the lower reaches. Background is hill-shaded topography derived from our 10 m surface DEM.

Figure 6: Supraglacial channel density calculated as the sum of pixels representing channels in 20 m grid-cells. Channel locations were defined as regions of the detrended surface DEM that were 0.025 m or greater below the detrended surface. Channel density is generally high at the eastern margin and the upper eastern region. Channel density is lowest in the western lower-glacier region. Background is hill-shaded topography derived from our 10 m surface DEM.

Figures

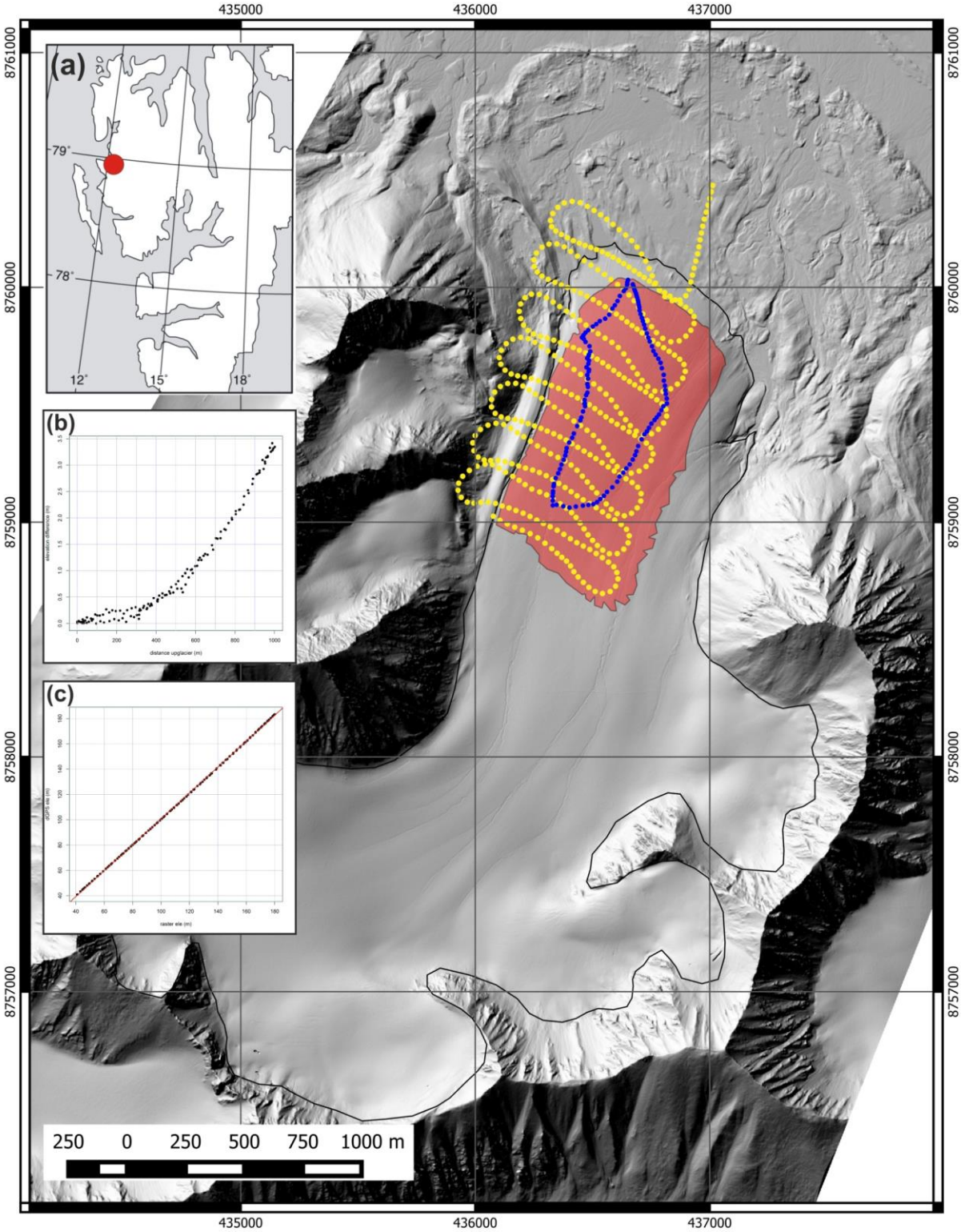

Figure 1: Hill-shaded 2.5 m Lidar-derived DEM of Midtre Lovénbreen, based on data collected in 2005 (after Arnold, N.S. personal communication). Pale-red shaded area represents the region covered in our 2013 survey. Yellow dots represent camera locations and dark-blue dots represent on-ice check-points. Inset (a) shows the location of Midtre Lovénbreen in Svalbard. Inset (b) shows how errors between dGPS-derived on-ice check points and our DEM increase upglacier. Inset (c) shows the relationship between surface elevations derived from our SfM-produced DEM and our dGPS on-ice check-points.

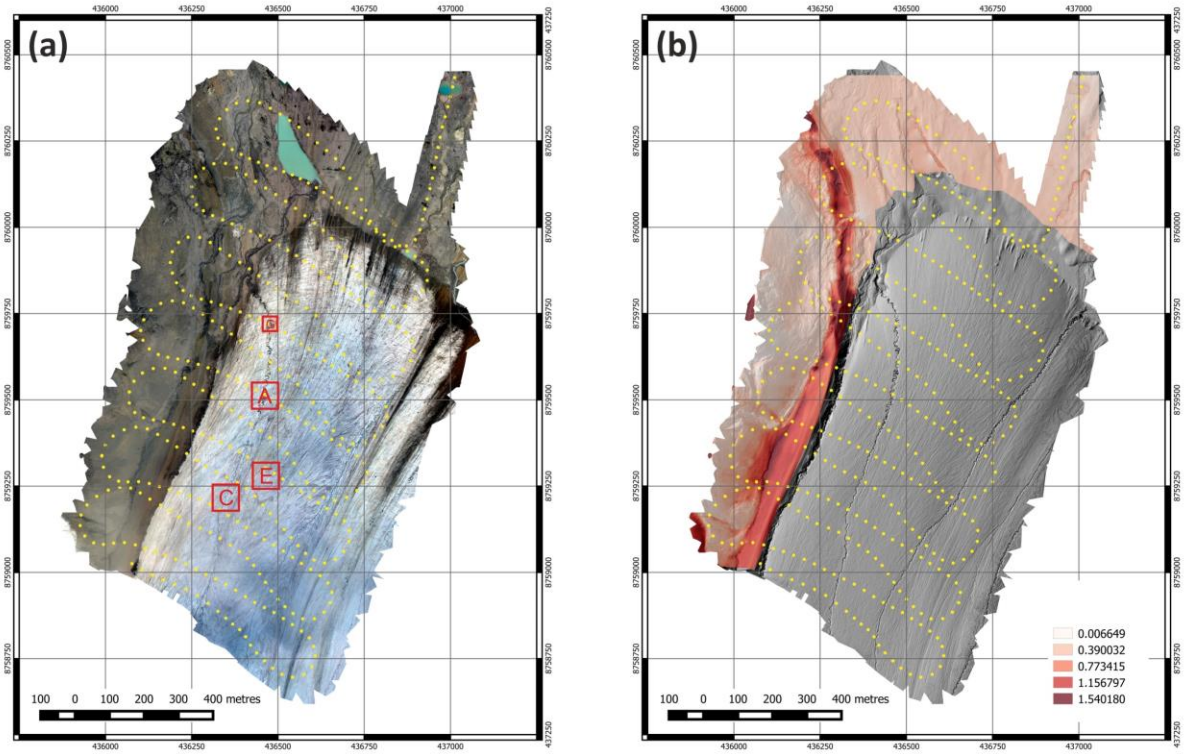

Figure 2: (a) Ortho-mosaic of the lower reaches of Midtre Lovénbreen. Mosaic created from 423 separate images collected during a single UAV flight. (b) Hillshaded digital elevation model derived from ortho-mosaic with a resolution of 10 cm. Both OM and DEM reveals spectacular detail with meandering supraglacial channels clearly visible and subtle surface features. On (b), the (red) shaded area represents the region of the forefield where our DEM elevations are compared with those of Irvine-Fynn et al. (2011). Elevation differences are expressed in metres per year. Positive change indicates surface lowering between 2005 and 2013. Yellow dots indicate camera locations. Red squares with letters on part (a) indicate locations of parts of Figure 3, such that 'A' indicated where Figure 3a (and associated part b) is derived from; 'C' indicates where Figure 3c (and associated part d) is derived from etc.

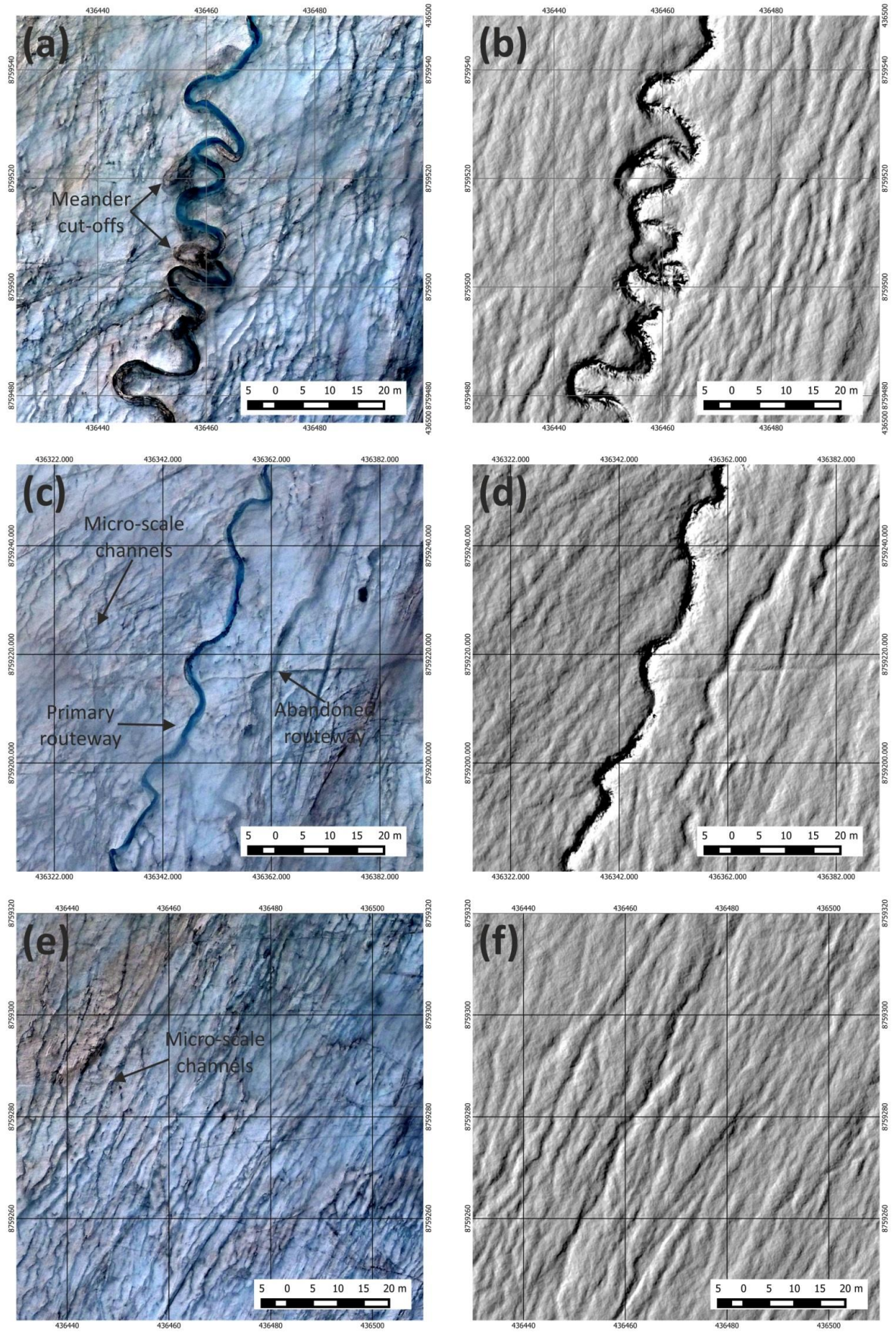
(a)
Meander cut-offs
(b)
(c)
Micro-scale channels
Primary routeway
Abandoned routeway
(d)
(e)
Micro-scale channels
(f)
5 0 5 10 15 20 m

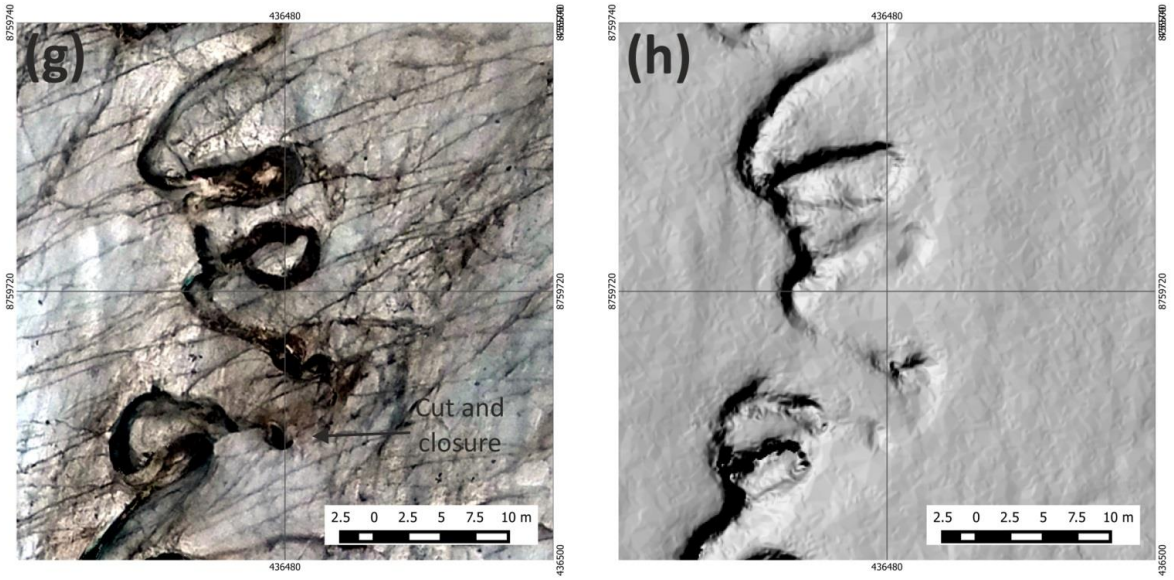

Figure 3: Parts a (OM) and b (DEM) show a section of the western primary channel where meander cut-offs are clearly evident. These are marked. Parts c (OM) and d (DEM) show a part of the western primary channel and an adjacent abandoned primary routeway. Parts e (OM) and f (DEM) show the extensive microchannel network. Parts g (OM) and h (DEM) show a potential region of cut-and-closure - i.e. where the ice surface has deformed over a once-supraglacial channel. Locations of each of these figures are marked on Figure 2a.

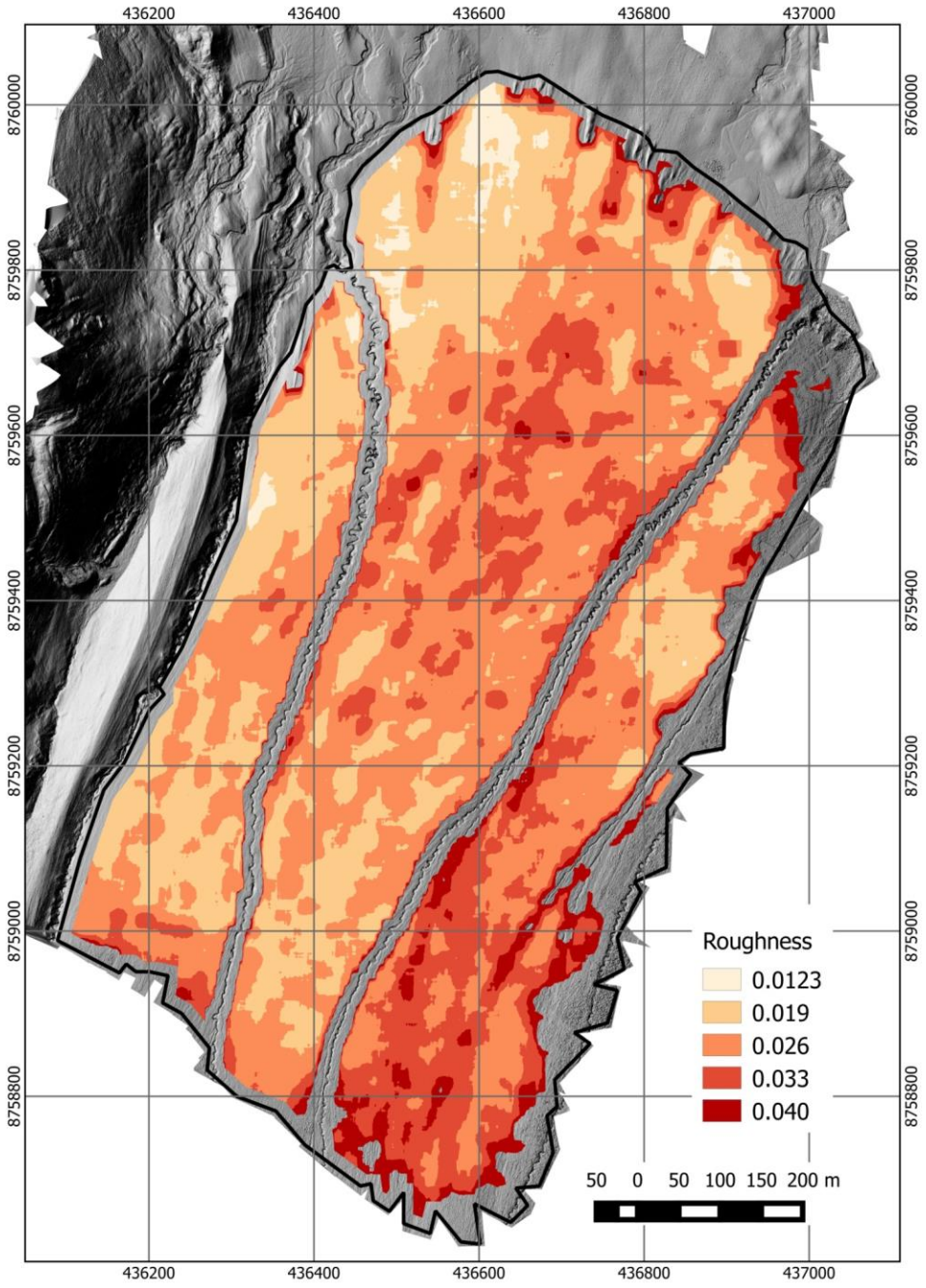

Figure 4: Surface roughness calculated as the standard deviation of detrended surface elevation in 20.5 m windows. Note how roughness is greatest in the upper-eastern reaches of the glacier, and lowest in the lower-western reaches. Background is hill-shaded topography derived from our 10 m surface DEM.

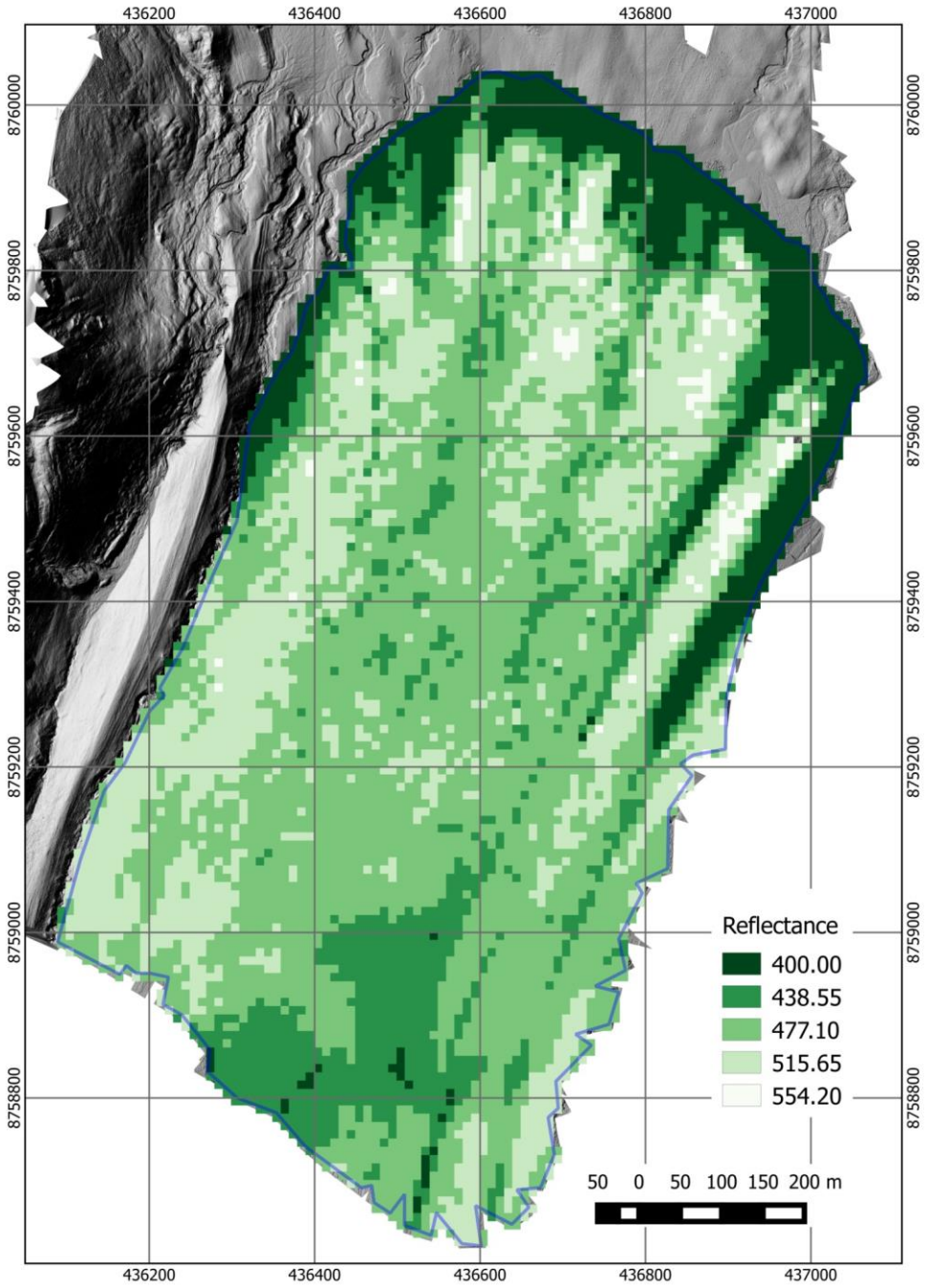

Figure 5: Surface reflectance calculated as the sum of the signal strength in the red, green and blue channels, as a crude proxy for albedo. These values were integrated over 10 m cells. Reflectance was lowest in the very lowest marginal areas (where debris cover is high). It was also low in the upper-eastern region of the glacier. Highest values are found close to the margins, particularly in the lower reaches. Background is hill-shaded topography derived from our 10 m surface DEM.

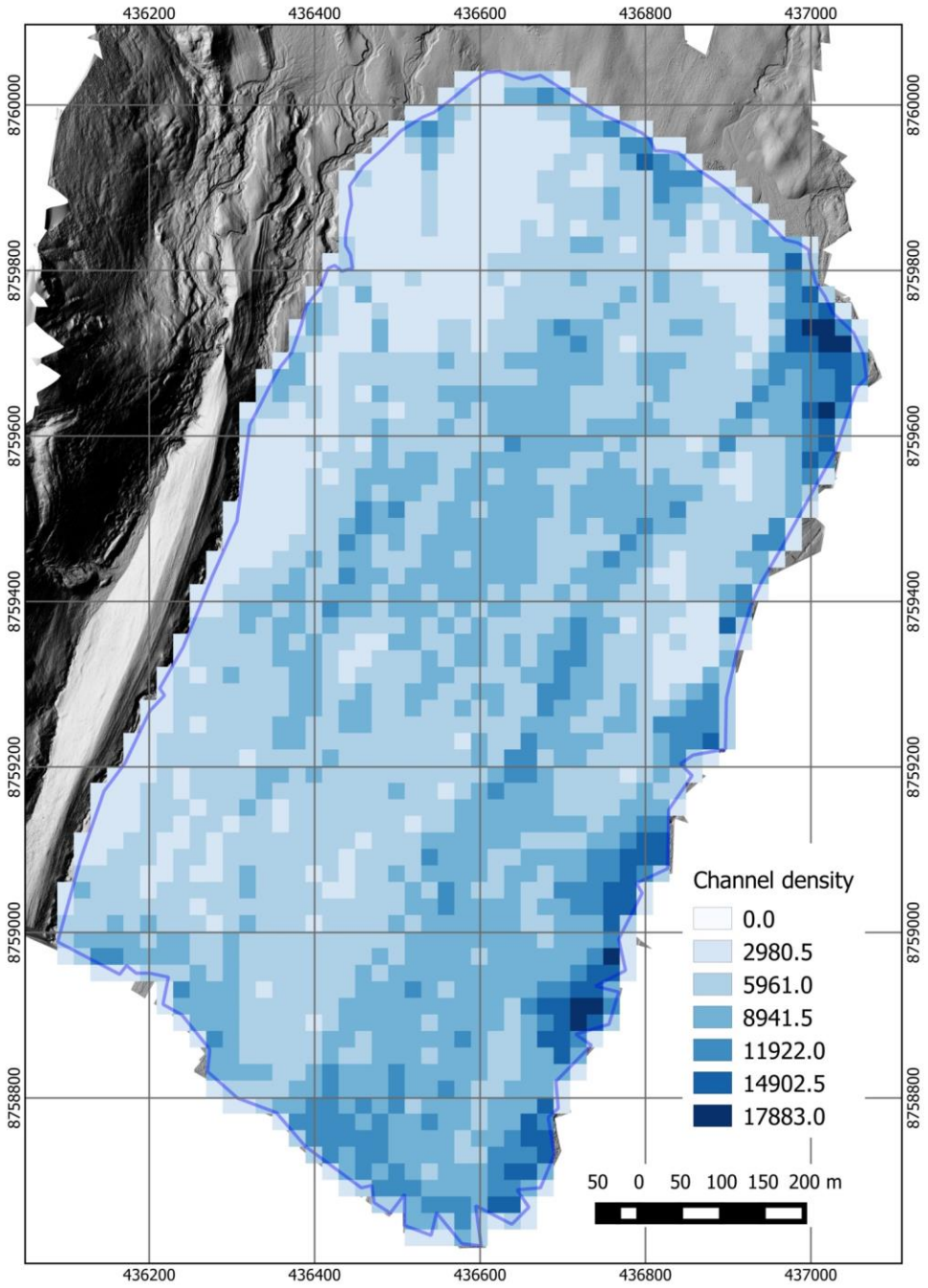

Figure 6: Supraglacial channel density calculated as the sum of pixels representing channels in 20 m grid-cells. Channel locations were defined as regions of the detrended surface DEM that were 0.025 m or greater below the detrended surface. Channel density is generally high at the eastern margin and the upper eastern region. Channel density is lowest in the western lower-glacier region. Background is hill-shaded topography derived from our 10 m surface DEM.